J Nanostruct 12(2): 426-445, Spring 2022

RESEARCH PAPER

Photocatalytic Degradation of Methylene Blue in Aqueous Solution with Silver-Kaolinite-Titania Nanocomposite under Visible Light Irradiation

Sudeshna Sharma [1], Arundhuti Devi [1], and Krishna Gopal Bhattacharyya [2]**

[1] *Institute of Advanced Study in Science and Technology, Department of Science &Technology, Guwahati, Assam, India*

[2] *Department of Chemistry, Assam Don Bosco University, Tapesia Gardens, Sonapur 782402, Assam, India*

ARTICLE INFO

Article History:
Received 29 December 2021
Accepted 18 January 2022
Published 01 April 2022

Keywords:
Ag-K-T Composite
Methylene Blue
Titanium Dioxide
Visible Light Photocatalysis

ABSTRACT

Silver-kaolinite-titanium dioxide (Ag-K-T) composite was synthesized and studied as a photocatalyst under visible light irradiation for degradation of the standard dye, Methylene Blue (MB). The catalyst was synthesized by mixing, pounding, pressurizing, grinding and calcining of Ag(I) nitrate with kaolinite and then combined with TiO_2 under certain specific environment and conditions. The characterization of the composite catalyst was done with XRD, FT-IR, SEM, EDX, TEM, AFM, TGA, CEC, BET, UV-DRS and PL analyses. The photocatalytic degradation was studied with process parameter variations such as catalyst loading, input dye concentration, pH of the medium and reaction time. The Ag-K-T composite had high cation exchange capacity (CEC) with large surface area and porosity. The aqueous dye ($5x10^{-6}$ M) was found to be 100% degradable with a catalyst loading of 0.5 g L^{-1}, reaction time of 70 min and at pH 7.5. The kinetics of dye degradation was also studied to find out the effectiveness of the photocatalyst. Chemical Oxygen Demand (COD) analysis of the aqueous dye solution before and after reaction confirmed degradation of the dye which was also observed through decolourisation. The photocatalyst was easily separable from the reaction mixture, could be regenerated and recycled successfully up to three cycles with decrease of only 1.68% of degradation rate. The work shows the potential of Ag-K-T photocatalyst to be used as a multifunctional material particularly with respect to decolourisation of wastewater containing dyes and pigments.

How to cite this article
Sharma S, Devi A, Bhattacharyya K G. Photocatalytic Degradation of Methylene Blue in Aqueous Solution with Silver-Kaolinite-Titania Nanocomposite under Visible Light Irradiation. J Nanostruct, 2022; 12(2):426-445. DOI: 10.22052/JNS.2022.02.018

INTRODUCTION

Dyes and pigments have been extensively employed in paper, paint, dyeing and textile industries and the treatment of the wastewater from these industries has always been a major environmental concern. The unused dyes impart aesthetically undesirable colour to the receiving water, reduce light penetration and often introduce toxic dyes and their intermediates into water [1]. Many of these dyes are harmful to the ecosystem and are considered as a significant hazard to aquatic living organisms [2]. Only 45-

* *Corresponding Author Email: kgbhattacharyya@gmail.com*

47% of the dyes are known to be biodegradable while others are insoluble, in many cases, harmful to human and other living beings, particularly due to their persistent quality. Many of the organic dyes are aromatic in nature and have carcinogenicity [3]. Methylene blue, the most commonly used cationic dye, has largely been used in textile and dyeing industry as well as in human and veterinary medicines. It cannot be degraded easily through the conventional routes of water treatment because of its complex aromatic structure, high stability against temperature, light, water and chemicals [4]. Many of the other dyes also resist degradation in conventional water treatment processes. It is important to formulate suitable strategies to efficiently remove the dues from industrial wastewater such that they do not harm aquatic life and do not enter into the human food chain. Usual treatment methods for dye degradation and removal include photocatalysis [5], adsorption [6], filtration and sedimentation [7]. All these processes have been seldom effective and the usual treatment processes are very much time-consuming. Advanced Oxidation Processes (AOP) like photo-Fenton, Fenton, ozonisation, semiconductor based photocatalysis have been developed for the effective degradation of dye pollutants [8]. Recently, the area of focus has shifted towards visible light photocatalysis, which is both cheap and environment-friendly and is modelled on the nature's process of utilization of sunlight for disinfection as well as degradation of various pollutants by utilizing cheap solar energy [9]. Photocatalysis is considered as a greener and economically beneficial approach in wastewater treatment based on strong oxidation and less energy consumption.

In recent years, TiO_2 has received considerable attention in wastewater treatment processes as a photocatalyst or photocatalyst-support as it has the advantages of being nontoxic, cost effective, and stable, with high photocatalytic efficiency for decomposition of persistent organic contaminants in water [10-14]. This oxide has a considerably vast band gap (3.12V) and can be used as a photocatalyst under ultraviolet (UV) irradiation. It has been observed that the photocatalytic efficiency of TiO_2 under visible light irradiation can be improved in a number of different ways, such as nonmetal doping [15], metal deposition [16] and semiconductor coupling [17, 18]. Doping of TiO_2 with silver (Ag^+), rubidium (Rb^+), nickel (Ni^{2+}), cobalt (Co^{2+}), copper (Cu^{2+}), vanadium (V^{3+}), ruthenium (Ru^{3+}), iron (Fe^{3+}), osmium (Os^{3+}), yttrium (Y^{3+}), lanthanum (La^{3+}), platinum (Pt^{4+}, Pt^{2+}), and chromium (Cr^{3+}, Cr^{6+}) has been shown to work splendidly under visible light as reported by Choi et al. [2]. Metal doping initiates a lower band gap externally that facilitates the electron–hole pair separation and hence increases active sites on TiO_2 surface [19]. For this purpose, Ag nanoparticles have been extensively studied because of their favourable optoelectronic properties. It is observed that the ideal size of Ag nanoparticles for use in photocatalysis is < 100 nm which prevents aggregation during the reactions resulting in macromolecule formation and in consequent reduction in the photocatalytic activity. To achieve this, the surface of Ag nanoparticles are stabilized with some surfactants or by immobilizing the nanoparticles over some supports such as metal oxides [8], carbon or alumina [20, 21]. To produce photocatalysts with desired functions, physical properties of the prepared material such as porosity, purity, surface area, surface aggregation and crystallinity have to be maintained at appropriate values. The properties are often influenced by the synthetic approach to the materials and their precursors. Several reports have pointed out that the kinetics of the reactions play an important role as the reaction rate relies on how the dye to be degraded is accumulating on the TiO_2 surface [22].

Clay-TiO_2 nanocomposites have been extensively reported because of their simple and environmentally benign process of synthesis. Incorporation of TiO_2 particles inside the silicate layers increases the specific surface area by resulting in a mesoporous structure with improved adsorbability [23]. Kaolinite ($Al_2O_7Si_2{\cdot}2H_2O$), a naturally occurring low cost and non-toxic, layer-structured aluminosilicate clay with presence of reactive hydroxyl groups is an outstanding support for introducing metal oxides within its framework structure and thus to prepare nanocomposites for various applications [24, 25]. Kaolinite has the added advantage as it does not show any swelling in water. The inter-lamellar space could be enlarged to the size required for accommodating nanoparticles by rupturing the hydrogen bonds interlinking the kaolinite lamellae. X-ray diffraction (XRD) measurements by Papp et al. indicated an increase in the basal spacing of the ordered structure of kaolinite from 0.72 to 1.12 nm as a

result of disaggregation of the metal particles protected in the inter lamellar space [26].

TiO_2 based photocatalysts have been usually prepared by using $TiCl_4$, $TiOSO_4$ and Ti(IV) alkoxides as precursors [27-29]. During the synthesis process, $TiCl_4$ shows volatility and dimerization behaviour which makes it difficult to handle even though it is a cost-effective precursor. Its alternatives, such as tetrabutylorthotitanate and titanium(IV) tetraisopropoxide are expensive and hazardous, hampering large-scale industrial production. However, these materials are the preferred Ti(IV)-source for preparation of TiO_2-based nanoparticles. The pore structure of the final product is directed by using surfactants or organic solvents.

In this work, silver kaolinite and titanium dioxide (Ag-K-T) composites were synthesized in an easy and cost-effective process and the material was characterized with respect to its structural, thermal, morphological and optical properties. Finally, the photocatalytic efficiency of the catalyst for methylene blue degradation was evaluated in aqueous medium under visible light irradiation.

MATERIALS AND METHODS

Materials

TiO_2 (99.8% metal basis, anatase, Sigma Aldrich, USA) and kaolinite (extra pure, Himedia, Mumbai) were taken as the starting materials. Silver nitrate and methylene blue were obtained from Merck Chemicals, Mumbai. Double distilled water (conductivity 0.15 $mScm^{-1}$) was utilized all through the investigations.

Preparation of the catalyst

Step1: Incorporation of silver in kaolinite

1.0 mmol of Ag(I) nitrate and 1.0 g kaolinite were disseminated in 500 mL distilled water and the mixture was stirred vigorously for 6 h in a magnetic stirrer (500 rpm) in dark (Fig.1). The mixture was kept undisturbed at 60 ºC in a hot air thermostat for 2 days. Then obtained precipitate was washed 3 times with distilled water and methanol to remove unreacted species, centrifuged and dried at 70 ºC [30]. The Ag(I) ions on kaolinite surface gets reduced to metallic silver by the action of mild reducing agent methanol [31].

Step 2: Modification of silver-kaolinite with Titanium dioxide

To get a powdered mixture comprising of 20% silver kaolinite and 80% TiO_2 the sample obtained from step 1 was weighed and ground with 4 times by wt. of TiO_2 for 30 min. Sample wafers were made by pressing it under 9-ton pressure in a hydraulic press. The wafers were calcined at 500 ºC for 3 h. The resulting material was granulated in a mortar to get a fine powder and was preserved for use as the catalyst. Silver and TiO_2 were likely to be present on the clay surface in an adsorbed state due to electrostatic force of interactions with the negatively charged clay surface.

Preparation of dye solution

The stock solution of concentration, 1.0×10^{-4} M was prepared by dissolving accurately weighed MB (mol. mass 319.85 g mol^{-1}) in double distilled water and was diluted to obtain the required dye solutions of concentrations, 1.0×10^{-5}, 5.0×10^{-5} and 5.0×10^{-6} M for the photocatalytic reactions.

Characterization techniques

FT-IR measurements were carried out with a Shimadzu FT-IR 3000 spectrometer. Powder XRD analyses were done with a Bruker D8 Advance diffractometer at diffraction angles of 5º to 80º (2θ) with step size of 0.039 (λ=0.154 nm). With a Perkin Elmer, TGA 4000 thermal analyzer system from 35 ºC to 800 ºC, thermo gravimetric analyses were conducted under a steady N_2 flow of 20 mL min^{-1} with a heating rate of 10º min^{-1}. The pore size, pore volume and specific surface area analyses were performed with a Autosorb iQ using BET isotherm and BJH equation methods. Bergaya and Vayer Method was used for calculation of the CEC of the samples [32]. Using $BaSO_4$ background, the solid UV-Vis diffuse reflectance spectrum was recorded with a Hitachi U4100 spectrometer at room temperature.

The photoluminescence spectrum of Ag-K-T was obtained on a fluorescence spectrometer (JASCO FP 8300 spectrofluorometer) with a xenon lamp as the source of excitation at room temperature. A scanning electron microscope (SIGMA 300) with an accelerated voltage of 5 kV, combined with an energy dispersive X-ray spectrometer (ELEMENT) microanalysis connection, was used to study the structure and elemental composition of Ag-K-T.

The TEM images were observed on a JEM-2100 Plus electron microscope equipped with an accelerating voltage of 200 kV. Parameters of roughness, topographic surface images and measurements of force modulation were obtained by means of atomic force microscopy (AFM)

(NTEGRA Prima, NT-MDT Technology) operated in semi-contact mode using rectangular silicon tip (force constant 18 Nm^{-1}). Averages of the measurements of roughness are taken from 5x5 and 10x10 μm^2 replication specimens using 1Hz scanning rate. Image and linear profiles were used to analyse the surfaces. The samples for the AFM study were treated for half an hour each by dispersing and sonicating Ag-K and Ag-K-T samples in distilled water (1 mg/100 mL) and placed on a microscopic cover glass accompanied by air drying.

The Zeta potential (ζ) analysis was carried out at 25 °C with 0.1 mg Ag-K-T sample ultrasonically dispersed in 10 mL of distilled water and measured in a Zetasizer Nano ZS90 (model no. ZEN3690). The pH was maintained from 3.0 to 10.0 by adding 0.1 M aqueous solutions of HCl and NaOH each.

The preparation of Ag-K-T is schematically shown in Fig. 1.

Photocatalytic reactions

The photocatalytic reactor (Fig. 2) consisted of a visible light source of tungsten lamp (250 W) with a wavelength filter (λ > 400 nm) (Philips 38941-1; PS 25, Frost-6100) fitted at the bottom of a stainless-steel chamber.

A double-walled beaker was used for the degradation experiments at room temperature. In order to establish an adsorption-desorption equilibrium, the reactants were shaken vigorously in the dark for half an hour before a photocatalytic reaction was carried out. 5 mL aliquots of the reaction mixture were taken out at 10 min intervals after irradiation of the reaction mixture and were analyzed for the unconverted dye in order to determine the kinetics of the photochemical reaction. The aliquots were centrifuged to separate the solid catalyst, if any and the concentration of the unconverted dye was determined by analyzing the centrifugate with a Shimadzu UV-1800 spectrophotometer (at λ_{max} = 664 nm). A set of blank reactions was also carried out without incorporating the catalyst following the same procedure. The dye degradation experiments were conducted for different dye concentrations of 5.0×10^{-6}, 1.0×10^{-5} and 5.0×10^{-5} M at pH 7.5 (pH of prepared dye solution) and a catalyst load of 0.1 g/200 mL. The influence of catalyst loading

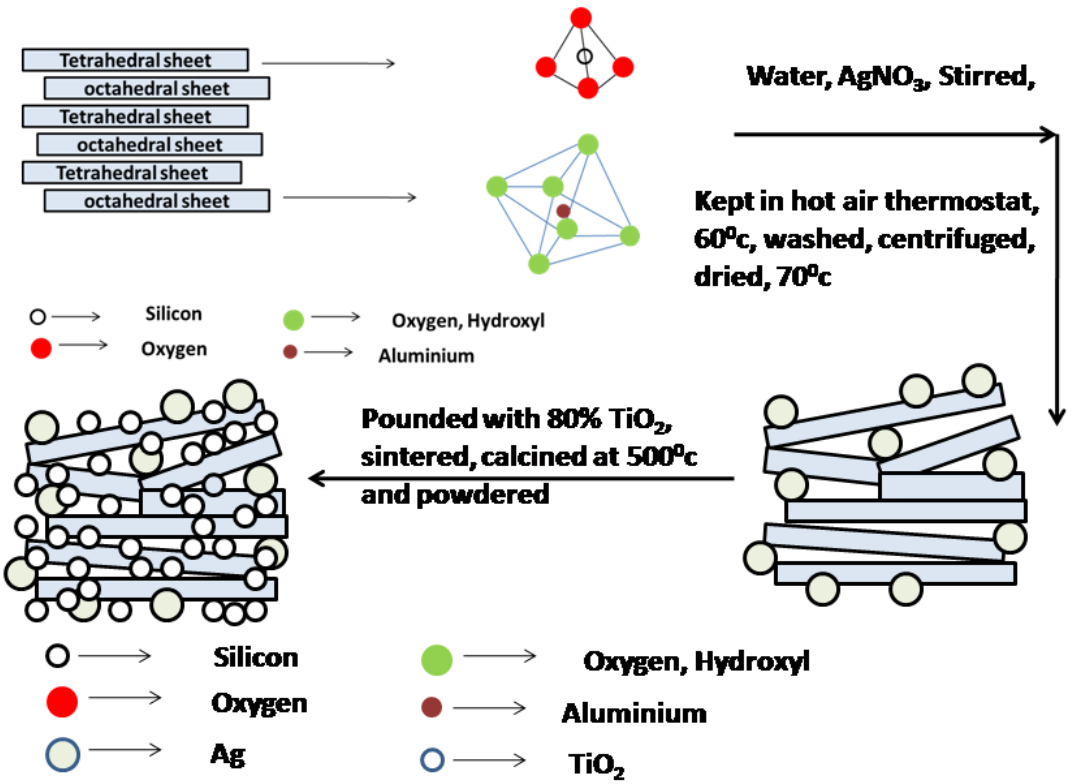

Fig. 1. Diagrammatic representation of preparation of Ag-K-T catalyst

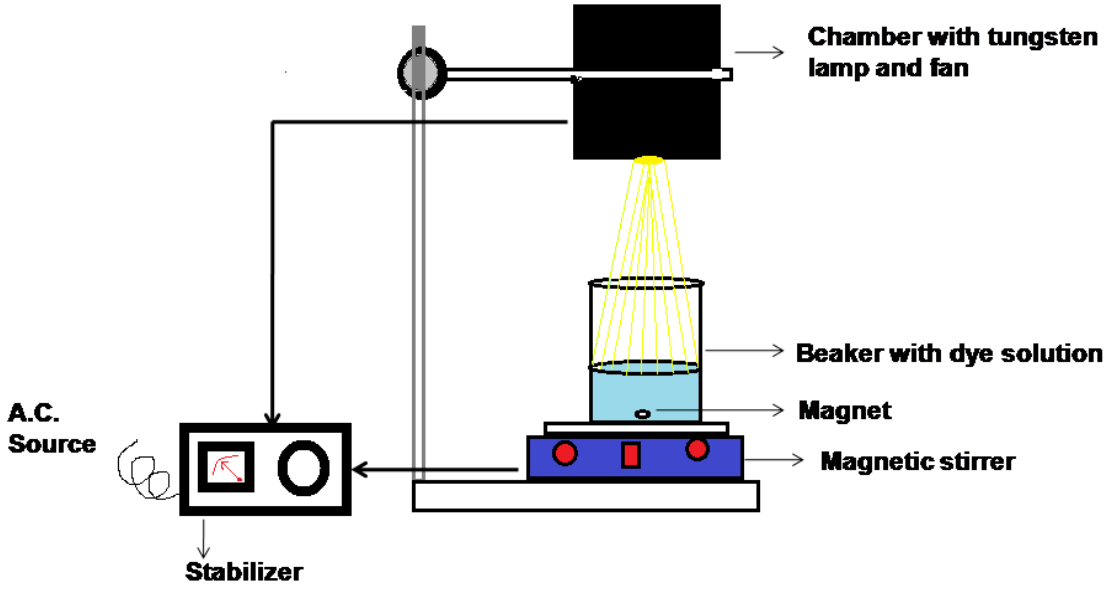

Fig. 2. Experimental set up for photocatalytic degradation of aqueous Methylene Blue under visible light

was studied with 0.005, 0.02, 0.04, 0.08 and 0.1 g catalyst/200 mL dye solution (concentration 1.0 × 10^{-5} M or 3.198 mg dye L^{-1}) at pH 7.5.

RESULTS AND DISCUSSIONS

Catalyst characterization

XRD analysis

The X-ray diffraction (XRD) patterns of Kaolinite (K), Titanium dioxide (T), Silver-Kaolinite (Ag-K) and the calcined Silver-Kaolinite-Titanium Dioxide (Ag-K-T) composite are shown in Fig. 3(a). The peaks located at 25.3, 36.9, 37.9, 48.2, 54.2, 55.3, 62.7, 68.8 , 70.4 and 75.3º (2θ) result from the tetragonal body centered anatase phase of TiO_2 and can be assigned to (101), (103), (004), (200), (105), (211), (204), (116), (220) and (215) planes (JCPDS file: 00-004-0477) and that located at 37.09 º (2θ) can be assigned to (101) diffractions of the hexagonal molecular Ag (JCPDS file: 01-087-0598) which is capped by (101) plane of Mg from kaolinite. Body-centred tetragonal Silicon and face-centered cubic aluminium from kaolinite produce the 38.6º band corresponding to (111) plane (JCPDS file: 01-074-6385). Characteristic peaks of kaolinite are observed at 2θ values of 12.27, 20.34, 25.06, 35.09, 38.65, 55.36 and 62.64º which can be assigned to (001), (110), (002), (130), (-110), (150) and (060) crystallographic planes [1].

Incorporation of water molecules, bound to each other as well as to the clay surface by inter-molecular hydrogen bonding, is responsible for expansion of basal spacing. Silver ions from silver nitrate will displace some of the water molecules and get adsorbed on the surface of the clay. Diffractions of Kaolinite (K) can still be observed clearly after calcination at approximately 500 ºC, indicating the retention of the layered structure of kaolinite (Fig. 3(a)). The XRD studies suggest that Ag-K-T composite has good thermal stability, further established by TGA analysis. The average crystal size of Ag-K-T composites was calculated using Scherrer–Debye equation [10] as

$$D = k\lambda / \beta \cos\theta \quad (1)$$

where D is the average size of the particles in nm, k is the shape factor constant (0.9), λ is the wavelength of X-rays (0.154 nm), β the broadening of the diffraction line measured by the full width at half maximum (FWHM) of the diffraction peak and Θ is the Bragg angle (in degrees). The average particle size of the Ag-K-T composite calculated from Scherrer–Debye equation as above was 34.88 nm in conformity with the formation of Ag-K-T nanoparticles (Fig. 3(c)).

FT-IR analysis

The FT-IR spectra recorded at room temperature for silver doped kaolinite (Ag-K) and silver doped kaolinite with Titanium dioxide composite (Ag-K-T) as compared with the parent kaolinite (K) showed the retention of layered structure of kaolinite in

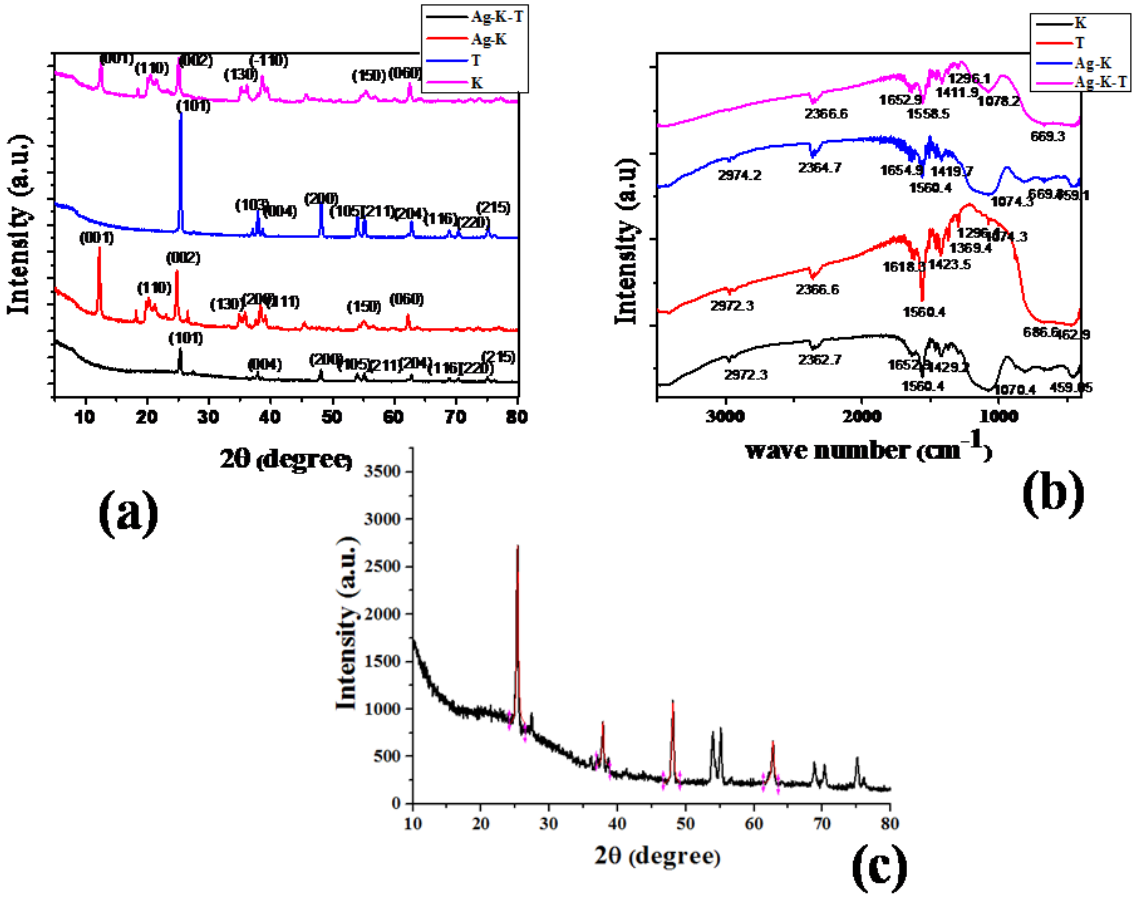

Fig. 3. (a) XRD pattern of Ag-K-T compared to Ag-K, T and K, (b) FT-IR spectra of K, T, Ag-K and Ag-K-T, (c) FWHM peaks considered for grain size calculation of Ag-K-T.

the prepared composites (Fig. 3(b)). The parent kaolinite showed characteristic absorption bands in the range of 3500–3700 cm^{-1} and 1000–1200 cm^{-1} (stretching of –OH and Si–O, respectively), weak bands between 900–400 cm^{-1} (Si-O-Si bending vibration) and absorption bands in 912–915 cm^{-1} range (-OH bending).

The bands at 500–650 cm^{-1} and 400–470 cm^{-1} could be assigned to the tetrahedral and octahedral complexes respectively. Therefore, in the investigated samples, the broad bands observed around 467 and 603 cm^{-1} were due to the stretching vibrations of the M–O bands in compounds where M denotes Si, Al or other cations existing in the sample. The bands at 2372 cm^{-1} and 3449 cm^{-1} were due to CO_2 stretching vibrations and H–O–H stretching vibrations respectively. The bands at 3420-3450 cm^{-1} could be due to H-O-H stretching of adsorbed water and that between 1620-1634 cm^{-1} due to H-O-H bending of water molecules. The bands near 1470 and 2850-2930 cm^{-1} can be assigned as C-H stretching bands [33, 34]. The IR spectra of the calcined catalysts in Fig. 3(b) indicates the substantial disappearance of Al–OH vibration bands. There is the formation of a broad band between 920 and 1280 cm^{-1} as a result of the superposition of Ti–O, Si–O and Al–O bands. After intercalation of Ag in the interlayer spaces of kaolinite, the intensity of the peaks of raw kaolinite changed. Some of the peaks present in kaolinite were masked due to TiO_2 impregnation and Ag doping and some were removed due to calcination of the modified clay [35, 36]. No additional peaks could be seen upon Ag-doping which indicates well dispersed doping ions [19].

Cation Exchange Capacity and Surface Area

The negatively charged sites present on

the surfaces of clay minerals can adsorb and hold cations by electrostatic force. The Cation Exchange Capacities of kaolinite and Ag-K-T composite were found to be 11.63 and 10.06 meq/100g respectively, using Bergaya and Vayer Method [32].

After introduction of metal cations and TiO_2 into the clay gallery, it was observed that the CEC of the parent clay decreased. This indicated the presence of some small ions within the interlayer space of the clay structure which introduces the negative interlayer charge. The decrease in the cation exchange capacity (CEC) of the clays following incorporation of the metal cations and TiO_2 is likely to be due to a concurrent loss of hydroxyl free radicals into solution. Calcination at 500 ºC for 3 h reduces the number of exchangeable cations and dehydroxylation of the polyoxo-cations is likely to liberate H_3O^+ ions within the clay bed [37].

The surface area, pore volume and pore radius of Ag-K-T were studied with BET and BJH adsorption and desorption cumulative analyses and were found to be 16.78 m^2/g, 0.15 cm^3/g and 17.72 nm respectively. As previously reported the surface area of the synthesized Ag-K-T catalyst was expectedly in between pure Kaolinite and pure TiO_2 [35-38]. After intercalation of Ag and TiO_2 particles on the silica layers followed by calcination, the specific surface area of the raw kaolinite decreases. This might be attributed to the increase in crystallite size due to grain growth and photocatalyst precipitation on silica particles during calcination and crystallization [39].

Thermogravimetric Analysis

The thermal stability of K, T, Ag-K and Ag-K-T was determined with TGA measurements (Fig.4). TGA readings of both Ag-K-T (already calcined at 500 °C) and parent TiO_2 are exactly the same which indicate almost the same thermal stability up to 750 °C. The TGA curves of kaolinite as well as Ag-K indicate a marginal weight loss at temperatures < 500 °C due to adsorbed water molecules. Dehydroxylation of water in the silicate layers as well as crystallization of TiO_2 causes weight loss at 460-670 ºC [40]. Since the crystal structure of kaolinite breaks down at temperature range of 550-650 ºC metakaolin is formed from calcination of kaolinite leaving an amorphous mixture of alumina and silica [41]. negligible weight loss is observed at temperatures ≥ 600 ºC indicating formation of a stable composite by calcination at these specific temperatures [35]. It is evident from

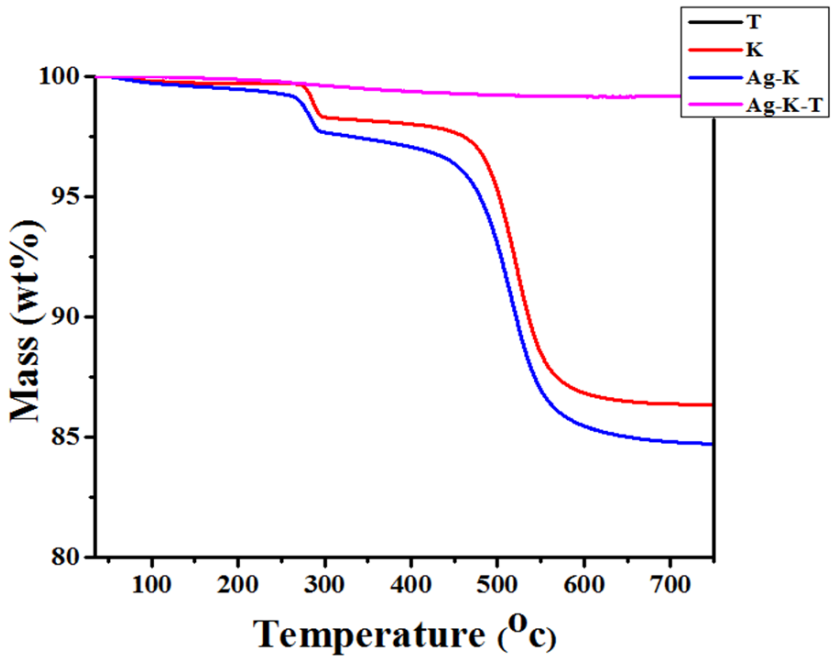

Fig. 4. Thermogravimetric analysis of K, T, Ag-K and Ag-K-T in the temperature range of 35° to 800 °C.

the TGA data that the Ag-K-T catalyst is thermally stable.

Scanning electron microscopy (SEM), Energy Dispersive X-ray (EDX), Transmission Electron Microscopy (TEM) and Atomic force microscopy (AFM) analyses

Surface morphology of the composite sample was investigated with SEM imaging measurements. The SEM images of the K, T, Ag-K and Ag-K-T are presented in Fig. 5(a). The morphology of pure kaolinite indicates the presence of plate-like structures. However, upon reaction with silver nitrate and TiO_2 the kaolinite structures were observed to get reduced to smaller particles containing spherical aggregates of TiO_2 [35]. Since the size of Ag is larger compared to the interlamellar space of kaolinite they get attached to the surface of kaolinite and some of them go into the interlayer space by deforming the parent kaolinite sheets. The interaction between TiO_2 and Ag-K lead to the formation of well distributed particles in Ag-K-T composites. Some of the plate-like structures of kaolinite were employed with Ag and stacking of the aggregates as well as deposition of TiO_2 on the surface was also observed. This leads to the formation of homogeneous photocatalysts.

Fig. 5(b) and 5(c) shows the X-ray mapping images and EDX spectrum of the Ag-K-T sample respectively. From the X-ray mapping images it can be said that the elements are well distributed on the surface which is a necessary criterion for a photocatalyst to be suitable for catalytic studies. Moreover, the EDX spectrum (Fig. 5(c)) of the sample demonstrates that the composite consisted of Ti, Ag, Si, Al, O and K atoms. Consequently, the surface became rough as shown by the AFM images of Ag-K and Ag-K-T (Fig. 7). The EDX data showed successful intercalation with 0.59% silver and 15.64% Ti in Ag-K-T sample (Fig. 5(c)).

The divergence of the metal contents from the measured CEC suggests the formation of a

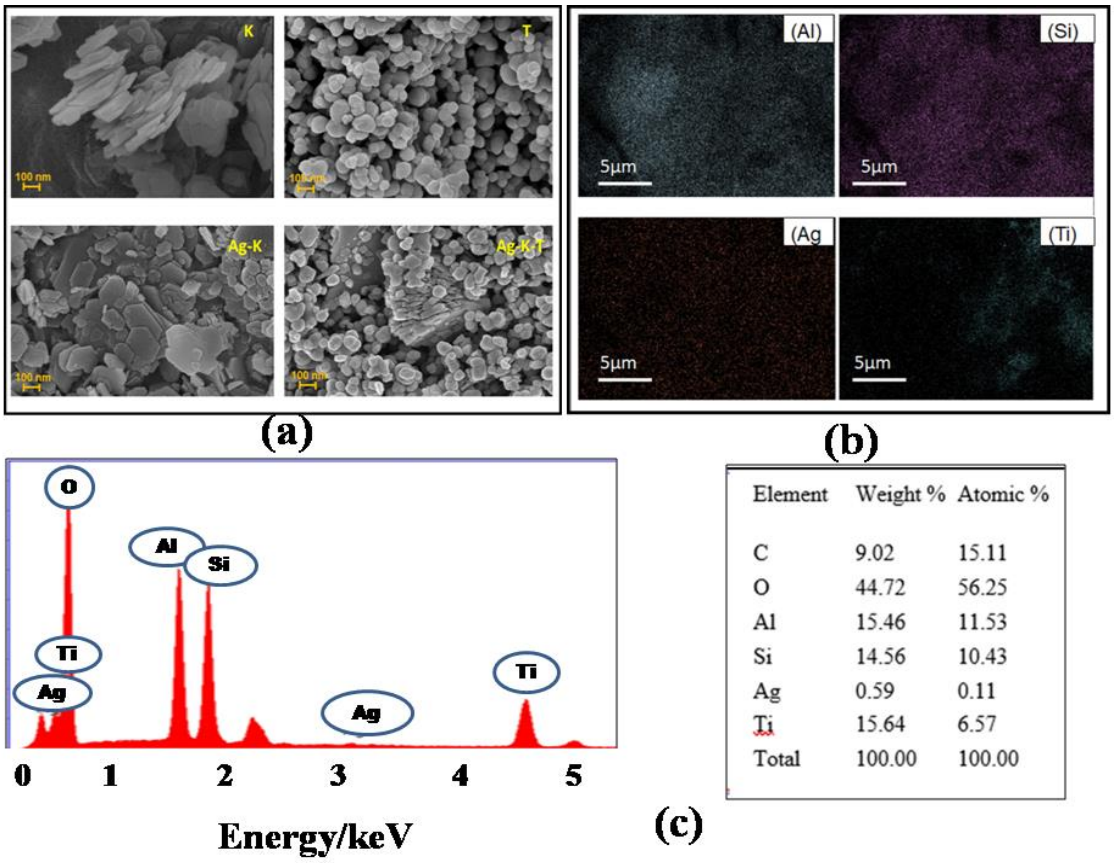

Element	Weight %	Atomic %
C	9.02	15.11
O	44.72	56.25
Al	15.46	11.53
Si	14.56	10.43
Ag	0.59	0.11
Ti	15.64	6.57
Total	100.00	100.00

Fig. 5. (a) Scanning Electron Microscope images of K, T, Ag-K and Ag-K-T (b) Elemental mapping image of Al, Si, Ag and Ti for Ag-K-T (c) EDX spectra and Elemental composition of Ag-K-T

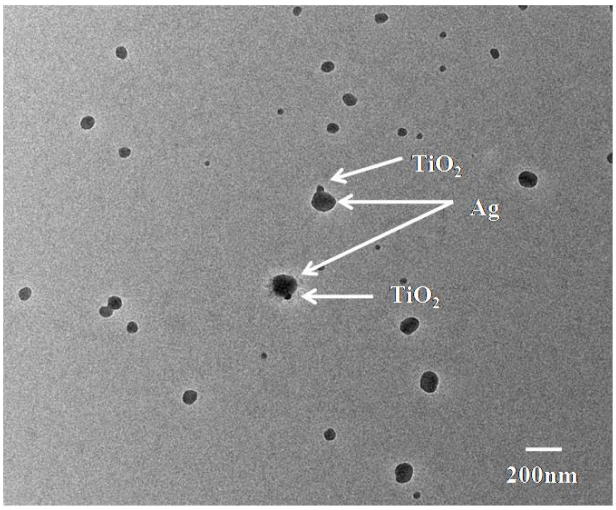

Fig. 6. TEM image of Ag-K-T

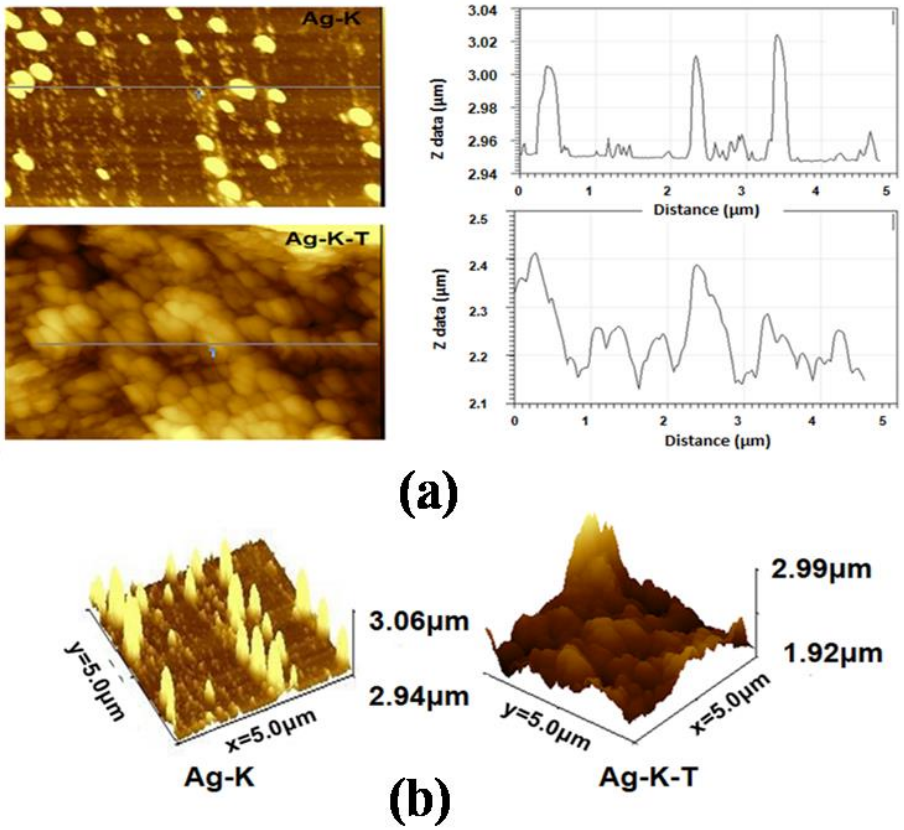

Fig. 7. (a) Surface topographic image and profile for Ag-K and Ag-K-T, (b)Three dimensional 5 µm^2 scans of surfaces demonstrating shape of surface features in relation to height for Ag-K and Ag-K-T

three-dimensional disordered structure called ''delaminated clay'' as most of the hydrolyzed titanium species and silver particles were observed to exist outside the clay interlayers and the polyoxycations co-aggregate with the clay particles [42].

Table 1. The surface roughness parameters of Ag-K and Ag-K-T from AFM analysis

Surface parameter	Ag-K	Ag-K-T
RMS roughness	14.47 nm	158.20 nm
Mean roughness	7.87 nm	128.60 nm
Minimum height	2.94 µm	1.80 µm
Maximum height	3.07 µm	2.81 µm
Median	2.95 µm	2.22 µm
Surface area	25.79 μm^2	32.36 μm^2
Volume	74.36 μm^3	56.21 μm^3

The distribution of TiO_2 and Ag nanoparticles can be observed in the TEM image (Fig. 6) where relatively larger Ag particles are surrounded by smaller TiO_2 particles and dispersed well on the kaolinite layer. On the basis of the structural analysis, a schematic diagram of the Ag-K-T composite was presented in Fig. 1. Because of the strong adsorption capacity of kaolinite, silver accumulates onto the clay surface after the addition of $AgNO_3$ into the kaolinite suspension. The subsequent addition of TiO_2 and calcinations facilitates formation of TiO_2 nanoparticles around metallic Ag on the surface of kaolinite.

AFM at magnification of (5 µm x 5 µm) showed different topographies with irregularly spaced and sized peaks (Fig. 7) for the two samples (Ag-K and Ag-K-T). Surface features of Ag-K-T indicated it to be of a larger, more rounded but shorter height appearance (Fig.7 (b)). The surface nano topography consisted of peaks and troughs with heights of the peaks ranging from 2.94 to 3.07 µm for Ag-K and from 1.78 to 2.81 µm for Ag-K-T. Three dimensional images after same z height correction indicates the differences in surface topography with Ag-K-T demonstrating an increased surface roughness compared to Ag-K (Table 1). The size of surface topographical features were observed to increase resulting in an increase in the surface area from 25.79 to 32.36 μm^2 and decrease in volume from 74.36 to 56.21 μm^3 for Ag-K and Ag-K-T respectively. Overall, the root mean square roughness of Ag-K increased from 14.47 nm to 158.2 nm for Ag-K-T, clearly pointing to good quality of the catalysts prepared [43]. Similar results have been observed by other workers by coating TiN and hydrated mineral surfaces with silver nanoparticles [44, 45].

Comparative UV-Vis DRS analysis

The optical measurements were performed at room temperature through UV-vis spectroscopy. Fig. 8(a) displays the optical absorbance spectra provided by titanium dioxide samples for pure and metal incorporated clay. The anatase TiO_2 polymorph has a band gap of about 3.22eV and is active under UV radiation with a wavelength of less than 387 nm [46]. Ag-K displays absorption close to 425 nm. Calcination at 500 °C allows the absorption core of the surface of Ag-K-T composite to change from approximately 425 to 450 nm. It has been noted that during high temperature calcination the growth of Ag nanoparticles occurs with the smoother Ag surface and smaller interparticle spacing between the TiO_2 anatase layer. These variations causes red shift of the surface plasmon absorption which is again stimulated by visible light [47]. Hence, the photocatalytic properties of TiO_2 are significantly enhanced [48]. Calcination at high-temperature results in the TiO_2 lattice being partially doped by the Ag species, although this doping would ultimately have an effect on the TiO_2 band structure and would therefore have an influence on photocatalytic activities under visible light [49].

When Ag-K-T composite was compared to pure TiO_2(T) significant red shifts with lower band energy of doped samples were observed due to Differences in surface conditions or doping effects on the structural and textural parameters of TiO_2 [19]. The red shift in the absorption spectra of modified TiO_2 with other transition metals is also being studied [28]. TiO_2 crystallizes around Ag on the surface of the kaolinite to form Ag-K-T nanocomposite.

Due to the surface plasmon resonance the Ag particles under visible-light irradiation get excited. Subsequently, the electrons excited by photons jump from the Ag particle surface to the TiO_2 conduction band. On the surface of TiO_2, O_2 molecules in the solution traps the injected

electrons from the Ag particles and superoxide ions ($O_2^{\bullet-}$) as well as other reactive species like •OOH, •OH are generated [50]. It is shown that the dye molecules could be oxidized by these oxidative species [51]. Further, holes generated by photons could also be present in the Ag atoms. The dissolution of Ag atoms through Ag^+ ejection would not have occurred due to the protection of the TiO_2 particles surrounding the Ag particles [52].

Band gap calculation

UV–vis absorption calculation is a simple and effective tool for describing the band structure of semiconductors. In order to better understand the semiconductive properties of Ag-K-T, the band gap between the prepared catalyst and that of pure anatase TiO_2 was calculated from solid UV–Vis diffuse reflectance analysis(Fig.8(b)) using the classical Tauc approach[19].

$$\alpha E_p = k\,(E_p - E_g)^n \qquad (2)$$

where E_g, E_p and k respectively represent the optical band gap, photon energy (hv) and a constant with the exponent, n, depending on the nature of transition. Values of n = 1/2, 3/2, 2, and 3 are taken for directly permitted, directly prohibited, indirectly permitted and prohibited transitions respectively.

The best fit of $(\alpha E_p)^2$ versus E_p was observed for n = 1/2 indicating allowed direct transitions through the energy band gap. For Ag-K-T, the extrapolated value of E_p at α = 0 supplies absorption edge energies of 2.9 eV (Fig. 8(a)). This value is much lower than that of pure TiO_2 (3.22 eV), which gives the prepared catalyst stronger semiconducting characteristics than pure TiO_2 under visible light

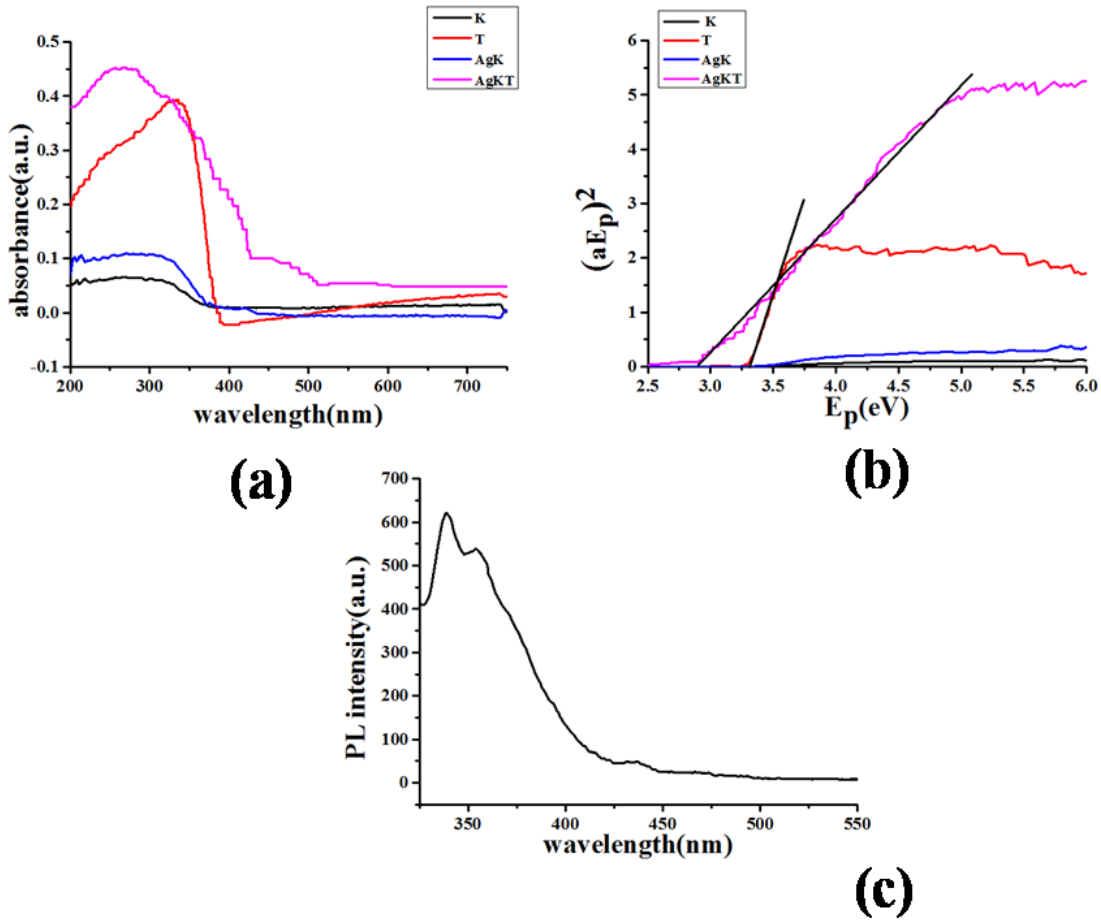

Fig. 8. (a) Diffused Reflectance Spectra of K, T, Ag-K and Ag-K-T (b) Comparative Band gap calculation from the reflectance spectra of T and Ag-K-T and (c) Photoluminescence spectra of Ag-K-T

range. Even though the composite is irradiated with long wavelength radiation, electron-hole pairs can be formed. Oxygen vacancies created causes a decrease in its band gap which are responsible for unique photocatalytic properties. Therefore, the Ag-K-T composite was expected to show greater activity in the visible region compared to pure TiO_2 and was therefore used under visible light for dye degradation[19, 28]. The band gap calculations were not shown for K and Ag-K samples as they are photocatalytically inactive (due to absence of TiO_2).

Photoluminescence analysis

Photoluminescence emission spectra have been used in semiconductors to consider the fate of electron–hole pairs in order to examine the efficiency of trapping, migration and movement of the carrier. The PL level would be lower if there is a lower e-h^+ recombination rate or a higher transfer of electrons and holes[10]. In the present work, PL technique is used to evaluate the optical properties, surface conditions, oxygen vacancy and defects present in the Ag-K-T composite. Incorporated photocatalytic systems display surface defects which result in significant excitonic PL emissions affecting photocatalytic activities [53]. Fig.8(c) displays the PL spectra of Ag-K-T under light excitation at λ_{ex} = 315 nm. It showed good PL emission intensities, suggesting the presence of either oxygen vacancy and/or defects that would lead to an increase in the material's optical properties by binding the photo-induced electrons easily to form excitons, so that the PL signal could be easily produced. High PL strength can occur due to the higher crystallinity of the Ag-K-T composite with lower defects [54]. Fig. 8(c) shows that when the composite is excited at 315 nm, multiple excitonic PL emission bands could be observed at 340, 356 and 437 nm resulting from the surface oxygen vacancy and defect of the sample. This observation is consistent with the findings of the UV-vis DRS spectra. Thus, the surface states and internal structures of the Ag-K-T composite are likely to play a critical role in their photocatalytic activities.

Photocatalytic reactions

When photons with higher energies than its band gap get incident on a semiconductor they get absorbed and the photocatalytic ability of the semiconductor changes according to its narrow band gap, surface area, light gathering ability and the rate of e^-–h^+ separation. High visible light photocatalytic activity can be obtained by production of more photo-induced carriers.

Comparative photocatalytic degradation of Methylene Blue

In these photocatalytic studies, 100 mg each of TiO_2 (T), silver-kaolinite (Ag-K) and silver-kaolinite-TiO_2 (Ag-K-T) was used in 200 mL aqueous solution of the dye and the mixture was stirred vigorously in a magnetic stirrer for 30 min in dark for establishing adsorption-desorption equilibrium and then irradiated by visible-light. The comparative photocatalytic degradation of the dye was in the order of Ag-K-T >Ag-K >T (Fig. 9(a)). It was observed that Ag-K sample could be an adsorbent but had negligible photocatalytic activity. Similarly, T could also be an adsorbent but has less photocatalytic activity under visible light because of extra absorption of light by TiO_2 at wavelengths > 400 nm or direct injection of electrons from the adsorbed dye molecules into the TiO_2 conduction band [2, 19].

Table 2. Degradation of aqueous Methylene Blue (1×10^{-5} M) at different Ag-K-T loadings

Loading (g)/200 mL dye solution	% Degradation of the dye
0.005	15.8
0.02	22.1
0.04	42.2
0.08	66.8
0.10	80.2

Table 3. Kinetic parameters for pseudo first order photocatalytic decomposition of aqueous Methylene Blue on Ag-K-T nanocomposite as well adsorption and photolysis study

Catalyst loading (g)/200mL	k_a (min^{-1})	R^2
0.005	0.001	0.941
0.02	0.002	0.910
0.04	0.004	0.994
0.08	0.009	0.978
0.1	0.015	0.928
0.1 (photocatalysis)	0.015	0.928
0.1 (adsorption)	0.006	0.994
0.1 (photolysis)	0.000	0.848

The degradation experiments were carried out one by one by varying the catalyst loadings, the concentration of the dye and the pH at different intervals of time (0 to 120 min). The photocatalytic degradation was measured by monitoring the concentration of the dye as a function of irradiation time at 10 min intervals (λ_{max} = 664 nm) using a UV-Vis spectrometer (Shimadzu 1800). The extent of dye decomposition was obtained from the equation

$$\% \text{ degradation} = (C_0\text{-}C)\ x100/C_0) \quad (3)$$

where, C_0 is the absorbance at time, t = 0 and C is the absorbance at a particular time interval. Upon increasing the irradiation time, the strong absorption bands of the dye decreased gradually. Dark reactions (in absence of light) and blank reactions (in absence of catalyst) were also performed under the same experimental conditions. Negligible degradation of the dye was observed in the absence of the photocatalyst.

Effect of photocatalyst loading

The influence of the catalyst amount on degradation of the dye under visible light using Ag-K-T catalyst was studied by varying the amount of catalyst as 0.005, 0.02, 0.04, 0.08 and 0.1g in 200 mL 1×10^{-5} M dye solution. The results showed that on increasing the catalyst loading from 0.025 to 0.5 g L^{-1}, an increase in decolorization efficiency was observed from 15.8 to 80.2% respectively. This is shown in Table 2. Further increasing the catalyst amount above 0.5g L^{-1} photocatalytic activity decreases because the nano composite catalyst particles in high concentration get aggregated in solution and act as barriers for the light irradiation [55]. The dye was rapidly decomposed at high catalyst loading. Thus, the availability of more and more adsorption sites with increasing catalyst loading (which in turn increases the rate of formation of hydroxyl radicals) led to rapid photocatalytic decomposition of the dye. This trend could also be attributed to the effect of Ag-nanoparticles on the surface of TiO_2/kaolinite and the formed Schottky barrier at the Ag/TiO_2 interface [56]. The results of fitting are shown in Fig. 9(b). Following this observation, the catalyst amount in subsequent photocatalytic degradation experiments was kept at 0.1g in 200mL dye solution.

Kinetics of photodegradation

The kinetics of degradation of methylene blue in aqueous solution (Fig. 9(c)) was studied under the optimum conditions (pH = 7.5; catalyst loading = 0.5 g L^{-1}; dye concentration = 1×10^{-5} M). The photocatalytic degradation of the dye followed pseudo-first-order kinetics, agreeing with the Langmuir-Hinshelwood model based on the equation:

$$\ln(C/C_0) = -\,kt \quad (4)$$

where, C is the concentration of the dye in mgL^{-1} at any reaction time and C_0 (mg L^{-1}) is the initial

Table 4. Effects of solution pH on photocatalytic degradation of aqueous Methylene Blue

pH	Zeta potential (mV)	Degradation efficiency, %
3.0	19.2	67.4
4.0	16.3	68.7
5.0	12.6	72.4
6.0	-21.5	78.3
7.0	-25.3	79.5
8.0	-24.5	82.2
9.0	-26.8	87.5
10.0	-29.3	94.8
11.0	-	96.7

concentration of the dye, k is the pseudo first order reaction rate constant, and t is the reaction time in min. The reaction rate constant increased from 0.001 to 0.015 min^{-1} when Ag-K-T loading was increased from 0.005 to 0.1 g/200 mL.

The kinetics for adsorption (in absence of light) and photolysis (in presence of light without catalyst) under similar conditions of pH, catalyst loading, temperature, reaction time and dye concentration were compared with those of the photocatalytic degradation (Fig. 9(c)). Some amount of adsorption was observed in the dark reaction, which could be attributed to the high surface area, porosity and CEC of kaolinite and titanium dioxide. However, the degradation of Methylene Blue under photolysis was negligible confirming that methylene blue is a stable dye in aqueous medium. The photocatalysis was observed to be the most efficient process among the three, i.e., $k_{photocatalysis} > k_{adsorption} > k_{photolysis}$ [57, 58].

The rate coefficients and R^2 values for the pseudo first order fitting of the reaction rate for different catalyst loadings (for 0.1 g catalyst / 200 mL dye solution) are given in Table 3.

Zeta potential analysis and effects of pH on photocatalytic degradation

The physicochemical properties of catalysts are influenced by pH (Table 4). In the present study, the pH of the prepared dye solution was 7.5, which was adjusted to any desired pH by adding 0.1 M NaOH or 0.1 M HCl dropwise. The other experimental conditions were kept constant at 0.1 g Ag-K-T loading/200mL of $1x10^{-5}$M aqueous Methylene Blue.

Fig. 9(d) demonstrates the impact of the initial pH of the reaction mixture on the photocatalytic degradation of Methylene Blue on Ag-K-T. The dye degradation was 67.4, 68.7, 72.4, 78.3, 79.5, 82.2, 87.5, 94.8 and 96.7% as the initial pH was varied from 3.0 to 11.0 (Table 4). Comparatively lower degradation was observed at acidic conditions and it steadily increased with increase in pH to the alkaline range.

The stability and surface charge of Ag-K-T nanocomposite was studied with zeta potential analysis by dispersing the sample in deionized water within pH range of 3 to 10 (Fig. 9(e)). The isoelectric point for the curve was found to be at pH 5.36 means below this pH the catalyst surface will carry a net positive charge and above it will have a net negative surface charge. When a metal oxide is dispersed in water, surface –OH groups can be protonated or deprotonated leading to surface charged ($-OH_2^+$ or $-O^-$) groups. The high negative value of zeta potential beyond isoelectric point indicates stability of the sample in water and low agglomeration. As Methylene Blue is a cationic dye, negative surface charge helps in attracting positive dye cations electrostatically and hence enhancing the adsorptive capacity resulting

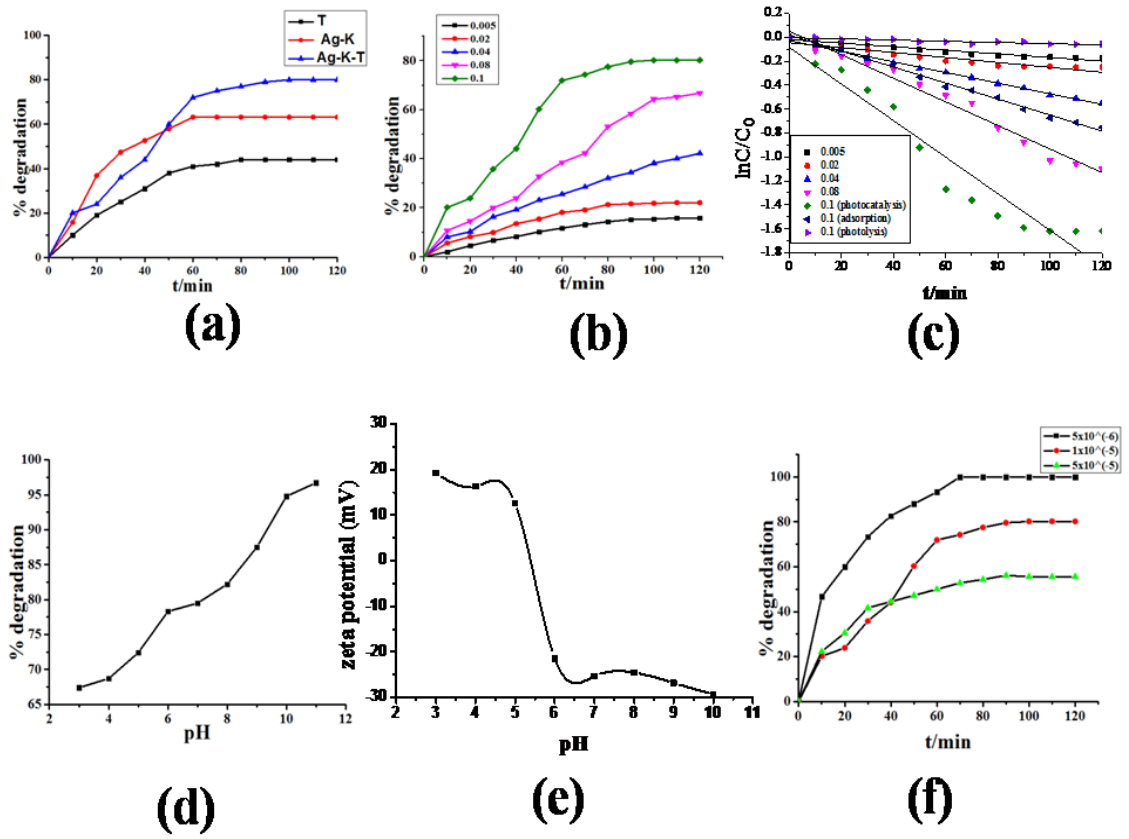

Fig. 9. (a) Comparative photocatalytic degradation of aqueous Methylene Blue with 0.5 gL^{-1} each of T, Ag-K and Ag-K-T for a reaction time of 120 min, pH 7.5 and dye concentration $1x10^{-5}$M, (b) The influence of catalyst loading on photocatalytic degradation of aqueous Methylene Blue with Ag-K-T under the same reaction conditions, (c) The fitting curve of pseudo-first-order kinetic equation and comparative study of photoctalysis, adsorption and photolysis, (d) Influence of initial pH on photocatalytic degradation of aqueous Methylene Blue with Ag-K-T under the same reaction conditions, (e) Zeta potential measurements of Ag-K-T at different pH values ranging from 3 to 10 (f) Influence on initial aqueous Methylene Blue concentration of $5x10^{-6}$, $1x10^{-5}$ and $5x10^{-5}$M with Ag-K-T loading of 0.5 gL^{-1}.

in high photocatalytic degradation of the dye [55, 59].

Influence of dye concentration on photocatalytic degradation of Methylene Blue

The effects of initial dye concentration were studied with dye concentration of $5x10^{-6}$, $1x10^{-5}$ and $5x10^{-5}$ M for a constant Ag-K-T loading of 0.5 g/L at pH 7.5 with 120 min irradiation time (Fig. 9(f)). As a general trend, the photodegradation efficiency of Ag-K-T decreased from 100% to 80.2% to 55.55% with increasing dye concentration (from $5x10^{-6}$ M to $1x10^{-5}$ M to $5x10^{-5}$ M). The key factor regulating the photodegradation of the dye is likely to be the formation of hydroxyl radicals on the surface of the catalyst as well as the interactions of these radicals with the dye molecules. For $5x10^{-6}$ M dye concentration, even in neutral medium, the degradation reaches 100% in 70 min. If the initial concentration of dye increases, far more dye molecules are adsorbed on the catalyst surface and thus the generation of hydroxyl radicals will decrease as the majority of the active sites are covered by the dye molecules. As a result, the efficiency of photodegradation decreased [5]. In addition, a shielding effect for light passing into solution is likely to be achieved at a high concentration of the dye, which in turn reduces the time to reach a maximum degradation efficiency at 90 min.

Similar findings have been reported and a few of these results are included in Table 5. Parameters such as pH, irradiation time, dye concentration, catalyst amount and % degradation

Table 5. Performance of a few photocatalysts for degradation of aqueous Methylene Blue

Catalyst	Light source	Irradiation time (min)	pH	Methylene Blue concentration (mgL^{-1})	Catalyst loading (gL^{-1})	% degradation	Ref
Ag@AgCl–TiO_2/sepiolite	Visible light	120	-	6	0.15	82.72	[27]
TiO_2–SiO_2/$CoFe_2O_4$	UV light	40	9	100	0.165	98.3	[28]
K-TiO_2	UV light	70	-	32	0.6	89	[35]
BN–Ag/TiO_2	Visible light	80		20	0.4	98	[10]
$NiWO_4$-reduced graphene oxide	Visible light	150	10	10	1	95	[21]
Fe_2TiO_5	Visible light	240	7	10	0.5	54	[55]
Ag_2O/TiO_2	Visible light	60	10	6.39	1	94	[61]
Fe_3O_4/$Ag_6Si_2O_7$	Visible light	2	10	5	0.1	98	[62]
Ag-K-T	Visible light	120	10	3.198	0.5	94.8	This work

of MB (aqueous) in the present work have been compared with other reported catalysts. The comparison shows that the synthesized Ag-K-T nanocomposite has strong potential to be used for photocatalytic degradation of aqueous methylene blue.

COD measurements

Chemical Oxygen Demand (COD) and Total Organic Carbon (TOC) analyses are widely used to study mineralisation of dye rather than using Biochemical Oxygen Demand (BOD) analysis as it is a very lengthy process and usually takes at least 3 days to complete an experiment. As the concentration of pollutants in industrial wastewater varies to a large extent, their analysis should be carried out rapidly and hence, 2 h COD analysis is a preferred one over lengthy BOD monitoring. Though TOC analysis takes lesser time (about 30 min) to complete, information obtained from it, is less useful as it cannot differentiate between two compounds with the same number of carbon atoms in different stages of reaction [60].

COD measurements in this work were done under acidic conditions (pH 4.5) by the closed reflux method using potassium dichromate as oxidant. The COD decreased from 58 mgL^{-1} to 18.56 mgL^{-1} (corresponding to 68% removal of the dye) which was supported by experimental photocatalytic removal of the dye. A remarkable decrease in COD implies efficient mineralisation of Methylene Blue with Ag-K-T composite.

Photocatalyst regeneration and reuse

The reliability, reusability and regeneration of a photocatalyst is a very significant economic factor for practical applications. To study the reusability of the catalyst, it was first centrifuged to separate from the reaction mixture, washed three times with distilled water and dried in a hot air thermostat at 70 ºC. Then it was used as a fresh catalyst for further reactions under the same conditions. The photocatalytic performance of Ag-K-T in the first three re-use cycles is shown in Fig. 10. The photocatalytic degradation rate decreased from 80.2% in the first run to 78.52% in the third run. Only 1.68% decrease in photocatalytic degradation was observed after the third run. The slight decrease may be due to the fact that

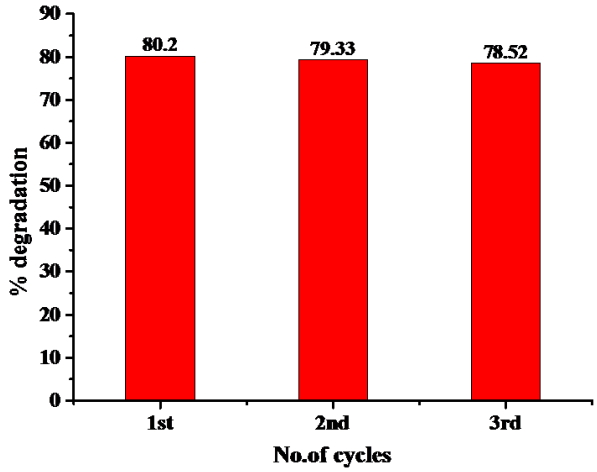

Fig. 10. Reusability of the photocatalyst for degradation of aqueous Methylene Blue

a little of the catalyst must have been washed off during the regeneration process, or that a few of the catalyst sites must have been occupied by some other constituents reducing slightly the efficiency of the catalyst, or there may have been some human or instrumental error in the measurements. Nevertheless, the findings suggest that Ag-K-T photocatalyst has excellent stability.

Mechanism of photocatalytic action

The mechanism of photocatalytic activity of the Silver-Kaolinite-Titania nanoparticles could be explained on the basis of energy band gap structure. The photocatalytic activity of Silver-Kaolinite-Titania could be attributed to the semiconductor property of TiO_2, while kaolinite as such does not have any photocatalytic activity. But it is a very good adsorbent for dyes and hence the modified semiconductor is supported on kaolinite for better surface adsorption of Methylene Blue and greater degradation. In pure TiO_2, the direct excitation of the electrons from the valance band (VB) to the conduction band (CB) is not possible in presence of visible light due to the wide band gap (3.21 eV). By integrating silver into the TiO_2 lattice, the TiO_2 band gap was decreased by introduction of impurity levels below CB in the band gap, such that the electrons could pass from VB to these energy levels leaving behind holes. These electrons travel to the surface and are adsorbed by O_2 and produce $\bullet O_2$ free radicals. On the other hand, holes created in the VB react with surface water or hydroxyl radicals to form strong redox species, •OH. These redox species are responsible for degradation of the dye cations adsorbed on surface [63-65]. Excitation of Methylene Blue molecules into singlet or triplet state with photons results in injection of electrons from the excited state to conduction band and hence an increase in hydroxyl and superoxide free radicals. This makes the photodegradation to proceed smoothly [66].

CONCLUSION

In this work, Silver-kaolinite-TiO_2 composites have been successfully synthesized as a less expensive, less toxic, environment friendly and efficient photo catalyst. The SEM images of the prepared catalyst compared to its raw materials (K, T) and step product (Ag-K) show successful intercalation and adsorption of Ag and TiO_2 in kaolinite mesoporous particles to form Ag-K-T nanocomposite, which is further confirmed by EDX data and particle size calculation from XRD analysis. AFM, BET and CEC measurements show higher specific surface area and grain size of Ag-K-T. Diffuse reflectance analysis confirms the red shift of the absorbance edge and decrease of the TiO_2 band gap value from 3.22 to 2.9 eV.

The photodegradation experiments with variation of catalyst loading, dye concentration and the pH of the reaction medium yielded results along the expected line. The results from variation of catalyst loading and subsequent kinetic study at constant pH of 7.5 and constant dye concentration of 1.0×10^{-5} M indicated that 0.5 g L^{-1} catalyst loading brings about the optimum 80.2% degradation of

the dye with pseudo first order kinetics yielding a rate constant of 0.015 min^{-1}. A comparative study of the three processes, photocatalysis, adsorption and photolysis, has shown a greater efficiency of photocatalysis in comparison to the others. The Langmuir-Hinshelwood mechanism has been useful for this comparison under similar reaction conditions. The catalyst acts at its maximum at basic pH range, which was confirmed by zeta potential measurements that indicated an isoelectric point at pH 5.36. All these results along with the environment-friendly nature of the nanocomposite and its less toxic quality indicate it to be a very strong, efficient multifunctional and promising photocatalyst for dyes like Methylene Blue in aqueous solution.

ACKNOWLEDGEMENTS

We would like to thank the Head, Chemistry Department, Gauhati University, for providing us the opportunity to carry out some experiments in the department. We would also like to acknowledge the kind cooperation of the Director, IASST, Guwahati for constantly supporting us with instrumental facilities.

CONFLICT OF INTEREST

The authors declare that there is no conflict of interests regarding the publication of this manuscript.

REFERENCES

1. Sarma GK, Sen Gupta S, Bhattacharyya KG. Removal of hazardous basic dyes from aqueous solution by adsorption onto kaolinite and acid-treated kaolinite: kinetics, isotherm and mechanistic study. SN Applied Sciences. 2019;1(3).
2. Choi J, Park H, Hoffmann MR. Effects of Single Metal-Ion Doping on the Visible-Light Photoreactivity of TiO_2. The Journal of Physical Chemistry C. 2009;114(2):783-792.
3. Devadi MAH, Krishna M, Murthy HNN, Sathyanarayana BS. Statistical Optimization for Photocatalytic Degradation of Methylene Blue by Ag-TiO_2 Nanoparticles. Procedia Materials Science. 2014;5:612-621.
4. Hou C, Hu B, Zhu J. Photocatalytic Degradation of Methylene Blue over TiO_2 Pretreated with Varying Concentrations of NaOH. Catalysts. 2018;8(12):575.
5. Reza KM, Kurny ASW, Gulshan F. Parameters affecting the photocatalytic degradation of dyes using TiO_2: a review. Applied Water Science. 2015;7(4):1569-1578.
6. Kausar A, Iqbal M, Javed A, Aftab K, Nazli Z-i-H, Bhatti HN, et al. Dyes adsorption using clay and modified clay: A review. J Mol Liq. 2018;256:395-407.
7. Sofianou M-V, Tassi M, Psycharis V, Boukos N, Thanos S, Vaimakis T, et al. Solvothermal synthesis and photocatalytic performance of Mn^{4+} -doped anatase nanoplates with exposed {0 0 1} facets. Applied Catalysis B: Environmental. 2015;162:27-33.
8. Botsa SM, Basavaiah K. Fabrication of multifunctional TANI/Cu_2O/Ag nanocomposite for environmental abatement. Sci Rep. 2020;10(1).
9. Zhang L, Yan J, Zhou M, Yang Y, Liu Y-N. Fabrication and photocatalytic properties of spheres-in-spheres ZnO/$ZnAl_2O_4$ composite hollow microspheres. Appl Surf Sci. 2013;268:237-245.
10. Nasr M, Soussan L, Viter R, Eid C, Habchi R, Miele P, et al. High photodegradation and antibacterial activity of BN–Ag/TiO_2 composite nanofibers under visible light. New J Chem. 2018;42(2):1250-1259.
11. Lee S, Lee Y, Kim DH, Moon JH. Carbon-Deposited TiO_2 3D Inverse Opal Photocatalysts: Visible-Light Photocatalytic Activity and Enhanced Activity in a Viscous Solution. ACS Applied Materials & Interfaces. 2013;5(23):12526-12532.
12. Yu Y, Xu D. Single-crystalline TiO_2 nanorods: Highly active and easily recycled photocatalysts. Applied Catalysis B: Environmental. 2007;73(1-2):166-171.
13. Ren Z, Hu X, Xue X, Chou K. Solid state reaction studies in Fe_3O_4–TiO_2 system by diffusion couple method. J Alloys Compd. 2013;580:182-186.
14. Yurdakal S, Palmisano G, Loddo V, Augugliaro V, Palmisano L. Nanostructured Rutile TiO_2 for Selective Photocatalytic Oxidation of Aromatic Alcohols to Aldehydes in Water. Journal of the American Chemical Society. 2008;130(5):1568-1569.
15. Yu J, Dai G, Huang B. Fabrication and Characterization of Visible-Light-Driven Plasmonic Photocatalyst Ag/AgCl/TiO_2 Nanotube Arrays. The Journal of Physical Chemistry C. 2009;113(37):16394-16401.
16. Teoh WY, Amal R, Mädler L, Pratsinis SE. Flame sprayed visible light-active Fe-TiO_2 for photomineralisation of oxalic acid. Catal Today. 2007;120(2):203-213.
17. Kansal SK, Singh M, Sud D. Studies on TiO_2/ZnO photocatalysed degradation of lignin. J Hazard Mater. 2008;153(1-2):412-417.
18. Akurati KK, Vital A, Dellemann J-P, Michalow K, Graule T, Ferri D, et al. Flame-made WO_3/TiO_2 nanoparticles: Relation between surface acidity, structure and photocatalytic activity. Applied Catalysis B: Environmental. 2008;79(1):53-62.
19. Khairy M, Zakaria W. Effect of metal-doping of TiO_2 nanoparticles on their photocatalytic activities toward removal of organic dyes. Egyptian Journal of Petroleum. 2014;23(4):419-426.
20. Botsa SM, Kumar YP, Basavaiah K. Facile simultaneous synthesis of tetraaniline nanostructures/silver nanoparticles as heterogeneous catalyst for the efficient catalytic reduction of 4-nitrophenol to 4-aminophenol. RSC Advances. 2020;10(37):22043-22053.
21. Botsa SM, Jagadeesh Babu M, Suresh P, Kalyani P, Venkateswararao B, Muralikrishna R. Spherical $NiWO_4$-reduced graphene oxide nanocomposite for effective visible light driven photocatalytic activity for the decolourisation of organic pollutants. Arabian Journal of Chemistry. 2020;13(11):8489-8497.
22. Mogyorósi K, Dékány I, Fendler JH. Preparation and Characterization of Clay Mineral Intercalated Titanium Dioxide Nanoparticles. Langmuir. 2003;19(7):2938-2946.
23. Liu J, Li X, Zuo S, Yu Y. Preparation and photocatalytic activity of silver and TiO_2 nanoparticles/montmorillonite

composites. Applied Clay Science. 2007;37(3-4):275-280.
24. Tokarský J, Čapková P, Burda JV. Structure and stability of kaolinite/TiO_2 nanocomposite: DFT and MM computations. J Mol Model. 2011;18(6):2689-2698.
25. Lu Z, Ren M, Yin H, Wang A, Ge C, Zhang Y, et al. Preparation of nanosized anatase TiO_2-coated kaolin composites and their pigmentary properties. Powder Technol. 2009;196(2):122-125.
26. Papp S, Szűcs A, Dékány I. Colloid synthesis of monodisperse Pd nanoparticles in layered silicates. Solid State Ionics. 2001;141-142:169-176.
27. Liu S, Zhu D, Zhu J, Yang Q, Wu H. Preparation of Ag@AgCl-doped TiO_2/sepiolite and its photocatalytic mechanism under visible light. Journal of Environmental Sciences. 2017;60:43-52.
28. Harraz FA, Mohamed RM, Rashad MM, Wang YC, Sigmund W. Magnetic nanocomposite based on titania–silica/cobalt ferrite for photocatalytic degradation of methylene blue dye. Ceram Int. 2014;40(1):375-384.
29. Zhang Y, Gan H, Zhang G. A novel mixed-phase TiO_2/kaolinite composites and their photocatalytic activity for degradation of organic contaminants. Chem Eng J. 2011;172(2-3):936-943.
30. Ménesi J, Kékesi R, Kőrösi L, Zöllmer V, Richardt A, Dékány I. The Effect of Transition Metal Doping on the Photooxidation Process of Titania-Clay Composites. International Journal of Photoenergy. 2008;2008:1-9.
31. Dong R-X, Chou C-C, Lin J-J. Synthesis of immobilized silver nanoparticles on ionic silicate clay and observed low-temperature melting. J Mater Chem. 2009;19(15):2184.
32. Bergaya F, Vayer M. CEC of clays: Measurement by adsorption of a copper ethylenediamine complex. Applied Clay Science. 1997;12(3):275-280.
33. Saikia BJ, Parthasarathy G, Borah RR, Borthakur R. Raman and FTIR Spectroscopic Evaluation of Clay Minerals and Estimation of Metal Contaminations in Natural Deposition of Surface Sediments from Brahmaputra River. International Journal of Geosciences. 2016;07(07):873-883.
34. Medhi H, Bhattacharyya KG. Retracted Article: Kinetic and mechanistic studies on adsorption of Cu(ii) in aqueous medium onto montmorillonite K10 and its modified derivative. New J Chem. 2017;41(22):13533-13552.
35. Shao GN, Engole M, Imran SM, Jeon SJ, Kim HT. Sol–gel synthesis of photoactive kaolinite-titania: Effect of the preparation method and their photocatalytic properties. Appl Surf Sci. 2015;331:98-107.
36. Wang C, Shi H, Zhang P, Li Y. Synthesis and characterization of kaolinite/TiO_2 nano-photocatalysts. Applied Clay Science. 2011;53(4):646-649.
37. Jobstmann H, Singh B. Water, Air, and Soil Pollution. 2001;131(1/4):203-215.
38. Sarma GK, Sen Gupta S, Bhattacharyya KG. Nanomaterials as versatile adsorbents for heavy metal ions in water: a review. Environmental Science and Pollution Research. 2019;26(7):6245-6278.
39. Ajenifuja E, Popoola API, Oyedotun KO, Popoola O. Microstructural and porosimetry analysis of Ag-TiO_2 intercalated kaolin and diatomite as nanocomposite ceramic materials. Clay Minerals. 2018;53(4):665-674.
40. Hilonga A, Kim J-K, Sarawade PB, Kim HT. Titania–silica composites with less aggregated particles. Powder Technol. 2009;196(3):286-291.
41. Johnson EBG, Arshad SE. Hydrothermally synthesized zeolites based on kaolinite: A review. Applied Clay Science. 2014;97-98:215-221.
42. Chen D, Du G, Zhu Q, Zhou F. Synthesis and characterization of TiO_2 pillared montmorillonites: Application for methylene blue degradation. Journal of Colloid and Interface Science. 2013;409:151-157.
43. Kumar M, Parashar KK, Tandi SK, Kumar T, Agarwal DC, Pathak A. Fabrication of Ag:TiO_2 Nanocomposite Thin Films by Sol-Gel Followed by Electron Beam Physical Vapour Deposition Technique. Journal of Spectroscopy. 2013;2013:1-6.
44. Whitehead K, Kelly P, Li H, Verran J. Surface topography and physicochemistry of silver containing titanium nitride nanocomposite coatings. Journal of Vacuum Science & Technology B, Nanotechnology and Microelectronics: Materials, Processing, Measurement, and Phenomena. 2010;28(1):180-187.
45. Brittle SW, Foose DP, O'Neil KA, Sikon JM, Johnson JK, Stahler AC, et al. A Raman-Based Imaging Method for Characterizing the Molecular Adsorption and Spatial Distribution of Silver Nanoparticles on Hydrated Mineral Surfaces. Environmental Science & Technology. 2018;52(5):2854-2862.
46. Aliou Guillaume PL, Chelaru AM, Visa M, Lassine O. "Titanium Oxide-Clay" as Adsorbent and Photocatalysts for Wastewater Treatment. Journal of Membrane Science & Technology. 2018;08(01).
47. Mulvaney P. Surface Plasmon Spectroscopy of Nanosized Metal Particles. Langmuir. 1996;12(3):788-800.
48. Awazu K, Fujimaki M, Rockstuhl C, Tominaga J, Murakami H, Ohki Y, et al. A Plasmonic Photocatalyst Consisting of Silver Nanoparticles Embedded in Titanium Dioxide. Journal of the American Chemical Society. 2008;130(5):1676-1680.
49. Rengaraj S, Li XZ. Enhanced photocatalytic activity of TiO_2 by doping with Ag for degradation of 2,4,6-trichlorophenol in aqueous suspension. J Mol Catal A: Chem. 2006;243(1):60-67.
50. Sung-Suh HM, Choi JR, Hah HJ, Koo SM, Bae YC. Comparison of Ag deposition effects on the photocatalytic activity of nanoparticulate TiO_2 under visible and UV light irradiation. J Photochem Photobiol A: Chem. 2004;163(1-2):37-44.
51. Viet PV, Phan BT, Mott D, Maenosono S, Sang TT, Thi CM, et al. Silver nanoparticle loaded TiO_2 nanotubes with high photocatalytic and antibacterial activity synthesized by photoreduction method. J Photochem Photobiol A: Chem. 2018;352:106-112.
52. Wu T-S, Wang K-X, Li G-D, Sun S-Y, Sun J, Chen J-S. Montmorillonite-Supported Ag/TiO_2 Nanoparticles: An Efficient Visible-Light Bacteria Photodegradation Material. ACS Applied Materials & Interfaces. 2010;2(2):544-550.
53. Cui G-J, Xu X-Y, Lin Y-J, Evans DG, Li D-Q. Synthesis and UV Absorption Properties of 5,5′-Methylenedisalicylic Acid-Intercalated Zn−Al Layered Double Hydroxides. Industrial & Engineering Chemistry Research. 2009;49(2):448-453.
54. Shyniya CR, Bhabu KA, Rajasekaran TR. Enhanced electrochemical behavior of novel acceptor doped titanium dioxide catalysts for photocatalytic applications. Journal of Materials Science: Materials in Electronics. 2017;28(9):6959-6970.
55. Vasiljevic ZZ, Dojcinovic MP, Vujancevic JD, Jankovic-Castvan I, Ognjanovic M, Tadic NB, et al. Photocatalytic

degradation of methylene blue under natural sunlight using iron titanate nanoparticles prepared by a modified sol–gel method. Royal Society Open Science. 2020;7(9):200708.
56. Kawahara K, Suzuki K, Ohko Y, Tatsuma T. Electron transport in silver-semiconductor nanocomposite films exhibiting multicolor photochromism. Physical Chemistry Chemical Physics. 2005;7(22):3851.
57. Mosleh S, Rahimi MR, Ghaedi M, Asfaram A, Javadian H, Sadeghfar F, et al. Visible-light-driven photocatalytic degradation of fenpyroximate in rotating packed bed reactor using Fe_3O_4@PbS@Ni_2P magnetic nanocomposite photocatalyst: Response surface modelling and optimization. Appl Organomet Chem. 2018;32(10):e4513.
58. Mosleh S, Rahimi MR, Ghaedi M, Asfaram A, Jannesar R, Sadeghfar F. A rapid and efficient sonophotocatalytic process for degradation of pollutants: Statistical modeling and kinetics study. J Mol Liq. 2018;261:291-302.
59. Azeez F, Al-Hetlani E, Arafa M, Abdelmonem Y, Nazeer AA, Amin MO, et al. The effect of surface charge on photocatalytic degradation of methylene blue dye using chargeable titania nanoparticles. Sci Rep. 2018;8(1).
60. Mohapatra S, Singh J, Satpati B. Facile synthesis, structural, optical and photocatalytic properties of mesoporous Ag_2O/TiO_2 nanoheterojunctions. Journal of Physics and Chemistry of Solids. 2020;138:109305.
61. Chen H, Chen N, Gao Y, Feng C. Photocatalytic degradation of methylene blue by magnetically recoverable Fe_3O_4/Ag6Si2O7 under simulated visible light. Powder Technol. 2018;326:247-254.
62. Dariani RS, Esmaeili A, Mortezaali A, Dehghanpour S. Photocatalytic reaction and degradation of methylene blue on TiO_2 nano-sized particles. Optik. 2016;127(18):7143-7154.
63. Oseghe EO, Ndungu PG, Jonnalagadda SB. Synthesis of mesoporous Mn/TiO_2 nanocomposites and investigating the photocatalytic properties in aqueous systems. Environmental Science and Pollution Research. 2014;22(1):211-222.
64. Benjwal P, Kar KK. Removal of methylene blue from wastewater under a low power irradiation source by Zn, Mn co-doped TiO_2 photocatalysts. RSC Advances. 2015;5(119):98166-98176.
65. Guan B, Yu J, Guo S, Yu S, Han S. Porous nickel doped titanium dioxide nanoparticles with improved visible light photocatalytic activity. Nanoscale Advances. 2020;2(3):1352-1357.
66. Pare B, Singh P. Reduction in Chemical Oxygen Demand and Color Intensity of Dye-Contaminated Wastewaster Using Visible Irradiation and ZnO-Assisted Advanced Oxidation Process: A Green Laboratory Experiment for Wastewater Treatment. Chemistry Education in the ICT Age: Springer Netherlands; 2009. p. 225-234.